Synthesis of stainless steel nanoballs via submerged glow-discharge plasma and its photocatalytic performance in methylene blue decomposition.

Muhammad Rafiq Mirza bin Julaihi[a], Shigeo Yatsu[a], and Seiichi Watanabe[a*]

[a]*Centre for Advanced Research of Energy and Materials, Faculty of Engineering, Hokkaido University, N13 W8, Kita-ku, Sapporo, Hokkaido 060-8628, Japan. Fax: +81-11-706-7886 Tel: +81-11-706-7886 *E-mail: sw004@eng.hokudai.ac.jp*

Synthesis of stainless steel nanoballs via submerged glow-discharge plasma and its photocatalytic performance in methylene blue decomposition.

Stainless steel nanoparticles or "nanoballs" have been synthesized using submerged glow-discharge plasma. Transmission electron microscopy showed that the nanoballs are uniformly spherical and size distribution estimation showed that their diameters are below 200nm. The decomposition of methylene blue solution under ultraviolet light with the wavelength of 354nm was observed in presence of stainless steel nanoballs. A mixture of stainless steel nanoballs and 0.1% methylene blue dye was irradiated with ultraviolet light. The concentration of methylene blue was reduced to baseline level in 72 hours. This shows that the stainless steel nanoballs have photocatalytic ability. In stainless steel nanoballs, methylene blue showed two different decomposition pathways; with a fast and slow reactions. Also, methylene blue was oxidized into sulfoxide before reducing into lighter byproducts. XRD analysis has shown that the nanoballs consist of Fe_2O_3 and Cr_2O_3, which are photocatalytically active species.

Keywords: stainless steel, nanoballs, photocatalytic, methylene blue

Introduction

Submerged glow-discharge plasma [1-8] has been researched as a method of nanoparticles synthesis. It is a process where plasma is produced by an electrical discharge in liquid. The product obtained after plasma electrolysis was found to be uniformly-shaped spherical nanoparticles called “nanoballs” [1]. As a result of

glow-discharge plasma causing localized melting spots on the cathode surface to occur repeatedly, molten material in order of nanosize became ejected from the cathode. Then they solidify into spherical nanoballs because of the surface tension and quenching effect of the electrolyte [1, 2, 8].

Nanoballs have good potential as photocatalytic materials because of their very small size and therefore high reactivity. Titanium oxide (TiO_2) and zinc oxide (ZnO) are well-known photocatalytic/photoelectric materials. Under ultraviolet (UV) light irradiation, TiO_2 and ZnO photocatalysts were able to decompose organic pollutants such as textile dye effectively [9-19, 20-25]. In the textile industry, waste materials such as excess dyes are contained in the discharged wastewater. The dyes in the wastewater pose a high risk to the ecosystem since they pollute the waterways. Therefore the research for other types of nanoparticle-photocatalyst besides TiO_2 and ZnO are also important not only for environmental cleaning, but also alternative energy production. Methylene blue dye was chosen as the indicator of photocatalytic performance because its decomposition is manifested as the decolourization of the dye. Furthermore, the concentration of the decomposition by-products can be measured using mass spectroscopy [33-35].

Stainless steel have been used as a photocatalytic material in its bulk form or

as a nanosized substrate for photocatalysts such as TiO_2. In its bulk form, the surface of stainless steel undergoes passivation and this layer was found to have photocatalytic ability when irradiated with UV light. As a substrate, stainless steel provides a stable surface and reduces the recombination rate in TiO_2. Despite the evidence showing the potential of stainless steel as photocatalytic materials, there has been no reports about the photocatalytic properties of stainless steel nanoparticles themselves. Typically stainless steel powders are synthesized using powder metallurgy via ball milling and vapor deposition technique [9-10].

The present research aims to synthesize stainless steel and also TiO_2 and ZnO nanoballs via submerged glow-discharge plasma. The stainless steel used is the JIS SUS316 (from here onwards referred as SUS), which contains iron, nickel and molybdenum. The nanoballs are characterized in terms of their physical characteristics (size, surface area, porosity, surface morphology) and photocatalytic performance. While there has been many reports on the photocatalytic ability of TiO_2 [9-18] and ZnO [20-25], there has been no report on the photocatalytic ability of SUS nanoballs. Furthermore, there are also no detailed reports concerning the synthesis of SUS nanoparticles as well. Since SUS nanoparticles contains potentially photocatalytically active oxides such as Fe_2O_3 and Cr_2O_3 [26-32], SUS nanoballs have good potential as a

photocatalytic material. A proposed mechanism of the photocatalytic ability of SUS nanoballs for methylene blue decomposition is also discussed in this paper.

Materials and Experimental Methods

Setup for submerged glow-discharge plasma

The nanoballs were synthesized via submerged glow-discharge plasma. **Figure 1** shows the experimental setup. A platinum wire of 1000mm in length, 0.5mm in diameter was used as the anode; this wire was bent and fixed onto a semicircular glass frame measuring 45mm in height and 60mm in width. A titanium/zinc/stainless steel wire of 1.0 mm in diameter and purity 99.99% mass (Nilaco, Tokyo, Japan) was used as the cathode. A glass tube was used as insulation to obtain an exposed length of 20 mm; the exposed part functioned as the net actual electrode. The electrolyte was a 300ml solution of 0.1 mol K_2CO_3 with 99.5% purity. The anode and cathode were dipped in solution of 10% sulphuric acid for a few seconds and then washed with purified water. The electrolyte was warmed until 90° Celcius, then electric current was applied until plasma forms under constant-voltage control (DC power supply: Takasago GP0250-10R). Then the voltage was fixed at a constant value for 3 hours. The sustained voltages for each type of electrode were 95V for Zn, 120V for Ti and 130V for SUS. **Figure 2** shows the voltage-current characteristics for the synthesis of SUS nanoballs.

Nanoballs collection and analysis method

After submerged glow-discharge plasma, the products were collected via centrifuging and washing with purified water to remove the electrolyte. Transmission electron microscopy (TEM, Hitachi H-700) images were taken at an operating voltage of 150kV and at 100,000 times magnification. Brunauer-Emmet-Teller (BET, Quantachrome Instruments Autosorb 6) method was used to measure the nanoballs' concentration, number per unit area, surface area and average size. The nanoballs were freeze-dried for 12 hours to convert the nanoballs into powder form. Scanning electron microscope-energy dispersive spectroscopy (SEM-EDS, JEOL JSM7001FA FE-SEM) was used to identify the elemental composition and mapping of each type of nanoball, using 15kV accelerating voltage. Size distribution software (Mac-View ver.4, Mountech Co. Ltd.) was used to estimate the nanoballs size distribution. X-ray diffraction (XRD, Rigaku Miniflex) was used to identify the elemental compositions and crystal structures of the nanoballs.

Photocatalytic test using MB and UV

The photocatalytic ability of the nanoballs was determined by the decomposition of methylene blue (MB). An aqueous solution of MB and nanoballs was exposed to ultraviolet (UV) irradiation for 24 hours while enclosed inside a dark chamber. The UV light was emitted at 354nm wavelength, and the power of the UV lamp was 100W. The

initial concentration of MB was 0.1g/1000ml. Ultra-violet/visible (UV/VIS) spectrophotometer (Jasco V-630) was used to measure the relative concentration of MB before and after the photocatalysis test. Before the photoabsorbance test, the UV-irradiated MB and nanoballs mixture were centrifuged to separate the MB solution from the nanoballs. By measuring the light absorbance of the MB, the transparency and subsequently the concentration of MB can be determined. Mass spectroscopy was used to determine the chemical compounds that were present after the photocatalysis test.

Experimental Results

Nanoballs have uniformly spherical shape

Figure 3 shows the TEM images of the nanoballs after glow-discharge plasma synthesis and centrifuging to remove K_2CO_3 electrolyte, while **Figure 4** shows the high-resolution transmission electron microscope (HRTEM) image of SUS nanoballs. From left to right are (A) TiO_2, (B) ZnO and (C) SUS respectively. In all three images, the nanoballs have uniformly spherical shape and are nanosized. It can be seen that the nanoballs size falls within a range of 50nm to 400nm, as confirmed by the particle size distribution and BET method. In terms of particle size uniformity, the size of ZnO nanoballs fell within a narrow range of 60nm to 150nm. In the case of SUS and TiO_2 nanoballs, their sizes fell within a wider range than those of ZnO nanoballs. For SUS

nanoballs, their sizes fell between 30nm and 300nm, while for TiO_2 nanoballs their sizes fell between 30nm and 400nm.

Increase in oxygen content in nanoballs

Figure 5(a) to **Figure 5(c)** shows the SEM-EDS results of the nanoballs, while Table 1 to Table 3 shows the elemental composition of the nanoballs and their parent materials. 1ml of the nanoballs in water was dropped onto a stainless steel plate, then the plates were dried prior to SEM-EDS observation. In **Figure 5(a)**, O atoms were detected alongside Fe, Mn, Ni, and Cr atoms on the surface of the SUS nanoballs.

Table 1 shows the elemental composition of SUS wire before submerged glow-discharge plasma, and the elemental composition of SUS nanoballs after submerged glow-discharge plasma. Before the application of plasma, SUS wire consisted of Fe, Ni and Cr atoms, which is consistent with the elemental composition of SUS316L. After the application of plasma, the nanoballs were found to contain O atoms in addition to Fe, Ni and Cr atoms of its parent material. These results indicate that the surfaces of SUS nanoballs were in their oxidized form after synthesis. In **Figure 5(b)**, O atoms were detected in addition to Zn atoms on the surface of ZnO nanoballs. **Table 2** shows the elemental composition of Zn wire and ZnO nanoballs. It is apparent that the amount of O has increased considerably in the case of ZnO nanoballs compared to its parent material.

In **Figure 5(c)**, O atoms were detected in addition to Ti atoms on the surface of TiO_2 nanoballs. **Table 3** shows the elemental composition of Ti wire and TiO_2 nanoballs. Similar to the case of SUS and ZnO nanoballs, after submerged glow-discharge, TiO_2 nanoballs were found to contain an increased amount of O atoms compared to Ti wire. Generally, for all three types of nanoballs, an oxide layer is thought to be present on the surfaces of the nanoballs. The oxide layer is evenly distributed on their surfaces. This oxide layer has an important role in photocatalysis, since they are reactive towards UV-light, releasing OH- free radicals. Since the oxide layer on the nanoballs has been identified, further investigation of the cross-sections of the nanoballs are needed. Also, the microstructure between the oxide surface and the nanoball bulk volume is of interest, to determine the growth mechanism of the oxide surface.

Presence of oxide nanoballs

Figure 6(a) to **Figure 6(c)** shows the XRD results of the nanoballs. In terms of peak intensities, FeO, Fe_2O_3 and Cr_2O_3 were the main characteristic peaks present in the case of SUS nanoballs. ZnO characteristic peaks were present in the case of ZnO nanoballs. Anatase and brookite TiO_2 characteristic peaks were present in TiO_2 nanoballs. The presence of Fe_2O_3 and Cr_2O_3 in SUS nanoballs contribute to its photocatalytic effect. The bandgap of Fe_2O_3 is 2.2eV, while the bandgap of Cr_2O_3 is 3.6eV. The low bandgap

of these oxides causes them to become photocatalytically active when irradiated with UV light. As a comparison the bandgap of anatase TiO_2 is 3.0eV, which is much higher than the bandgap of Fe_2O_3 and Cr_2O_3. Even though the bandgap of the oxides in SUS nanoballs were lower than the bandgap of anatase TiO_2, SUS nanoballs decomposed MB at a slower rate than anatase TiO_2. The decomposition behaviour of MB in presence of SUS, ZnO and TiO_2 nanoballs are shown in the photoabsorbance test results.

Table 4 shows the BET results of the nanoballs. ZnO nanoballs had the largest surface area and pore volumes of all three types of nanoballs, nearly double than the values measured on TiO_2 nanoballs. The large surface area of ZnO nanoballs was consistent with its excellent photocatalytic ability, where it was able to decompose MB in a relatively short time compared to TiO_2 and SUS. Although SUS nanoballs had the lowest surface area and pore volume compared to ZnO and TiO_2 nanoballs, the measurements indicate that the surface area and pore volume of SUS similar to that of TiO_2 nanoballs.

Photoabsorbance shows MB concentration decrease after UV

Figure 7(a) to **Figure 7(c)** shows the photoabsorbance test results after MB decomposition in presence of nanoballs. MB peak intensity was reduced by mixing with these nanoballs while UV-light was irradiated onto the photocatalytic test setup. **Figure 7(b)** shows the absorbance in case of ZnO nanoballs present in the mixture of MB. The

characteristic peaks of MB at 290nm and 650nm became lower than initial height after UV irradiation, indicating decomposition of MB has occurred. The characteristic peaks of MB were also reduced in intensity in case of SUS and TiO_2 nanoballs, shown in **Figure 7(a)** and **Figure 7(c)**. MB was effectively decomposed in presence of all three types of nanoballs. ZnO decomposed MB the fastest, followed by TiO_2 and SUS nanoballs. Mass spectroscopy showed that for TiO_2 and ZnO nanoballs, MB was decomposed directly into lighter molecules within 24 hours.

The decolouration of MB was calculated relative to the initial concentration of untreated MB solution (0.1g/1000ml). In the case of TiO_2 and ZnO nanoballs, MB peaks decreased drastically to almost baseline level after 24 hours of UV-irradiation. The decrease shows that the concentration of MB has decreased after UV-irradiation in presence of nanoballs. The decrease in concentration is caused by the photocatalytic decomposition of MB into simpler compounds, as a result of the UV-irradiation acting on the nanoballs. In the case of SUS nanoballs, MB peak decreased to baseline level after 72 hours of UV-irradiation, which was much longer than in case of TiO_2 and ZnO nanoballs.

Mass spectroscopy shows MB decomposition byproducts

Figure 8(a) to **Figure 8(c)** shows the mass spectroscopy results of the decomposition of MB. According to their mass charge ratio (m/z), the by-products of MB decomposition

can be identified. Generally the intensities of MB (m/z = 284.13) were reduced in all three types of nanoballs. Mass spectroscopy has shown that by-products such as phenol (m/z = 94.93), benzenosulfonic acid (m/z = 152.92), Azure A (m/z = 236.08) and Azure B (m/z = 271.20) were detected after UV-light irradiation. This showed that decomposition of MB has occurred in presence of the nanoballs while UV-irradiation was applied.

Discussion

In case of ZnO and TiO_2 nanoballs, the decomposition process occurred in a straightforward manner. Over the period of 24 hours, MB was gradually decomposed into lighter products. This was evidenced by the appearance of the peaks of MB by-products in the sixth hour graphs. At 24 hours, the peak of MB did not appear in ZnO. In case of TiO_2, the peak of MB at 24 hours still appeared, but its concentration was greatly reduced compared to before UV-irradiation. In case of SUS nanoballs, the decomposition process occurred differently compared to ZnO and TiO_2. First it was oxidized into sulfoxide (m/z: 301.15), then it was reduced/decomposed into lighter products. Additionally, methylene blue decomposed into different by-products at six hour and 24 hour UV-irradiation respectively. This process is evidenced by the above mass spectroscopy data, where the sulfoxide peak appeared in the sixth hour graph. The rest of the peaks however are similar to the peaks that appeared in case of

decomposition occurring in ZnO and TiO_2 nanoballs. After 24 hours of UV-irradiation, the peak of MB did not appear, while the peak for sulfoxide still increased. At the same time, the peaks of the decomposition by-products have also increased.

In case of SUS nanoballs, MB was decomposed to more simple molecules via oxidation into sulfoxide because of the photocatalysis effect. Within 24 hours, MB was oxidized into sulfoxide. When UV-irradiation was continued up to 72 hours, sulfoxide then reduced into lighter by-products without reverting into MB. This showed that SUS nanoballs were able to decompose the dye solution, although it took a longer time than TiO_2 and ZnO nanoballs. Also, the mechanism in which MB was decomposed was different compared to the decomposition mechanism in TiO_2 or ZnO. The decomposition of MB was confirmed in the photoabsorbance test of SUS nanoballs. Therefore, these results indicate that SUS nanoballs also have photocatalytic activity when irradiated with UV-light.

During the synthesis of nanoballs, size control was achieved by modifying the glow-discharge voltage. Higher glow-discharge voltage generally produced smaller sized nanoballs, while lower glow-discharge voltage produced larger sized nanoballs. This is shown in the case of TiO_2 and SUS nanoballs, where higher glow-discharge voltage produced small-sized nanoballs. For TiO_2, the maximum voltage that can be applied was 150V, and for SUS 160V. In the case of ZnO, voltages between 100V and

135V produced flower-like nanoparticles, whereas the optimal voltage for spherical nanoball production was 95V [2]. However there is a limit to the maximum voltage than can be applied; once this limit is exceeded arc-discharge plasma appears and melts the electrode immediately. Other than voltage control, the nanoballs can be separated according to size by using different-sized filters. There were relatively few microsized particles present after collecting the nanoballs. These are thought to be synthesized because of the irregularities of the plasma current flow.

Optimization of nanoballs synthesis is needed to produce smaller sized nanoballs with larger surface area; BET measurement shows that submerged glow-discharge has good potential to produce nanoballs with large surface area. It is evident from the XRD and photoabsorbance results that only small amounts of Fe_2O_3 and Cr_2O_3 are present in SUS nanoballs. The small amount of photocatalytically active oxides in SUS nanoballs causes SUS nanoballs to exhibit photocatalytic effect at a lower activity compared to TiO_2 and ZnO nanoballs.

Figure 9 shows the proposed mechanism for MB decomposition in presence of our synthesized nanoballs. The reaction that methylene blue underwent in its decomposition in presence of SUS nanoballs is unique compared to the reactions in presence of TiO_2 or ZnO nanoballs. In TiO_2 and ZnO, MB was decomposed directly into products with lower mass number. However, in presence of SUS nanoballs, MB

was oxidized into sulfoxide (m/z: 301.15) first, then decomposed into lighter products without reducing into MB again.

It is expected that O_2 and O^- were consumed during the photocatalytic reaction of MB in presence of SUS nanoballs. O_2 and O^- most likely originated from the surface of SUS nanoballs, where MB molecules were attracted towards the surface because of the charge difference between the MB molecules and the SUS nanoballs surface. After oxidation into sulfoxide, photocatalysis process reduces sulfoxide into lighter products. At this stage, free radicals ($O^{\cdot}$ and OH^-) attacked the bonds of MB and sulfoxide, severing the bonds, thus decomposing MB and sulfoxide into lighter products. Also, because methylene blue decomposition showed two different pathways, we suppose that there is a bottleneck effect between six hours and 24 hours UV-irradiation. This effect caused the SUS nanoballs to react to different bonding sites in MB at different times.

In case of TiO_2 and ZnO, O_2 has been consumed during the formation of the nanoballs from its parent materials, namely Ti and Zn. Therefore, no available O_2 existed for oxidation of MB into sulfoxide.

Stainless steel was shown to become an active catalyst under certain conditions. Di Mondo et al. (2011) reported that 316 grade stainless steel reactor wall became an active catalyst under acidic conditions and elevated temperature [38]. They observed the deoxygenation of glycerol and levulinic acid when it is flowed into the reactor. The

phenomenon was attributed to the synergistic effects between Fe, Ni and Cr that involved hydrogen spillover effects between sites that activate H_2(g) and sites responsible for hydrogenation steps.

In our research, SUS nanoballs became activated photocatalyst under UV irradiation. MB was found to become decomposed in presence of all three types of nanoballs and in UV irradiation.

The results indicate a new discovery of MB decomposition pathway occurring in a nonsemiconductor material, namely SUS nanoballs. The reactivity of SUS nanoballs is due to its large surface area and reactivity of Fe_2O_3 and Cr_2O_3 as a light-sensitive material. Previous reports have shown that rust (which contained Fe_2O_3) acted as a photocatalytic material to accelerate the corrosion of stainless steel when exposed to sunlight [29], and that the passivation layer on the surface of stainless steel (which contained both Fe_2O_3 and Cr_2O_3) exhibited semiconductive behaviour [30]. However the amount of the photocatalytically active species in SUS nanoballs is still lacking compared to those in TiO_2 or ZnO. Further research is needed to increase the amount of those active species.

The advantages of submerged glow-discharge plasma for nanoballs synthesis are: (1) simple experimental setup, (2) ease of control of nanoball sizes, (3) ease of mass production because of relatively high yield, and (4) use of easily available metallic

wires as raw materials for nanoballs synthesis. It is important to find other types of nanoparticles besides TiO_2 that exhibit photocatalytic activity. Other materials that can be synthesized via submerged glow-discharge plasma include virtually all metallic elements and alloys. Theoretically, if glow-discharge plasma can be sustained using a metallic electrode, nanoballs can be synthesized.

Conclusions

SUS, TiO_2 and ZnO nanoballs have been successfully synthesized via submerged glow-discharge plasma. Submerged glow-discharge plasma easily synthesized alloyed nanoballs. This research has demonstrated the photocatalytic performance of the nanoballs, especially in the case of SUS nanoballs, where it was able to effectively decompose MB. The presence of photocatalytically active species such as Fe_2O_3 and Cr_2O_3 was confirmed in SUS nanoballs. In SUS nanoball case, MB decomposition occurred in two pathways; fast and slow decomposition. MB was observed to oxidize into sulfoxide before being reduced into lighter byproducts. This is different compared to the MB decomposition pathway occurring in presence of TiO_2 and ZnO nanoballs. In the case of TiO_2 and ZnO nanoballs, MB reduced into lighter by-products without being oxidized into sulfoxide first.

References

[1] Toriyabe Y., Watanabe S., Yatsu S., Shibayama T., Mizuno T. Controlled formation of metallic nanoballs during plasma electrolysis. Appl Phys Lett. 2007; 91: 041501-1-3.

[2] Saitou G., Hosokai S., Akiyama T. Synthesis of ZnO nanoflowers by solution plasma. Mater Chem Phys. 2011; 130: 79-83.

[3] Moon SY, Han JW, Choe W. Feasibility study of material surface treatment using an atmospheric large-area glow plasma. Thin Solid Films. 2006; 506-507: 355-359.

[4] Parkansky N, Frenkel G, Alterkop B, Beilis I, Boxman RL, Barkay Z, Rosenberg Y. Ni-C powder synthesis by a submerged pulsed arc in breakdown mode. J Alloys Compd. 2007; 464: 483-487.

[5] Bogaerts A, Neyts E, Gijbels R, van der Mullen J. Gas discharge plasmas and their applications. J. Spectrochim Acta Part B. 2002; 57: 609-658.

[6] Qiao WM, Song Y, Lim SY, Hong SH, Yoon SH, Mochida I, Imaoka T. Carbon nanospheres produced in an arc-discharge process. Carbon. 2005; 44: 187-190.

[7] Xu Z, Liu X, Zhang P, Zhang Y, Zhang G, He Z. Double glow plasma surface alloying and plasma nitriding. Surf Coat Technol. 2006; 201: 4822-4825.

[8] Denaro AR, Hickling A. Glow-Discharge Electrolysis in Aqueous Solutions. J Electrochem Soc. 1958; 105: 265-270.

[9] SkySpring Nanomaterials, Inc. [Internet] Stainless Steel Nanoparticles [cited 2013 Jun 24]. Available from: http://www.aculon.com/particles-stanless-steel.php

[10] Aculon Performance Surface Solutions. [Internet] Stainless Steel Particle Coatings & Stainless Steel Nano Particle Treatments [cited 2013 Jun 24]. Available from: http://ssnano.com/inc/sdetail/stainless_steel_nanoparticles/2760

[11] Fujishima A, Rao TN, Tryk DA. Titanium dioxide photocatalysis. J Photochem Photobiol C Photochem Rev. 2000; 1: 1-21.

[12] Zhang JZ. Metal oxide nanomaterials for solar hydrogen generation. MRS Bull. 2011; 36: 48-55.

[13] Fujishima A, Honda K. Electrochemical Photolysis of Water at a Semiconductor Electrode. Nature 1972; 238: 37-38.

[14] Gopal KM, Shankar K, Paulose M, Varghese OK, Grimes CA. Enhanced Photocleavage of Water Using Titania Nanotube Arrays. Nano Letters 2004; 5: 191-195.

[15] Fernandez A, Lassaletta G, Jimenez VM, Justo A, Gonzalez-Elipe AR, Herrmann JM, Tahiri H, Ait-Ichou Y. Preparation and characterization of TiO_2 photocatalysts supported on various rigid supports (glass, quartz and stainless steel). Comparative studies of photocatalytic activity in water purification. Appl Catal B. 1995; 7: 49-63.

[16] Gnaser H, Orendorz A, Ziegler C, Rowlett E, Bock W. TOF-SIMS study of photocatalytic decomposition reactions in nanocrystalline TiO_2 films. Appl Surf Sci. 2006; 252: 6996-6999.

[17] Horikiri S, Teshima N, Saruki Y, Nishikawa H, Sakai T. Decomposition of methylene blue by new porous photocatalysts and analysis of decomposed products using high-performance liquid chromatography and mass spectrometry. Bunseki Kagaku. 2003; 52: 881-885.

[18] Lakshmi S, Reganathan R, Fujita S. Study on TiO_2-mediated photocatalytic degradation of methylene blue. J Photochem Photobiol A Chem. 1995; 88: 163-167.

[19] Kwon CH, Shin H, Kim JH, Choi WS, Yoon KH. Degradation of methylene blue via photocatalysis of titanium dioxide. Mater Chem Phys. 2004; 86: 78-82.

[20] Ha JW, Do YW, Park JH, Han CH. Preparation and photocatalytic performance of nano-TiO_2-coated beads for methylene blue decomposition. J Ind Eng Chem. 2009; 15: 670-673.

[21] Mozia S, Toyoda M, Inagaki M, Tryba B, Morawski AW. Application of carbon-coated TiO_2 for decomposition of methylene blue in a photocatalytic membrane reactor. J Hazard Mater. 2007; 140: 369-375.

[22] Saitou G, Hosokai S, Tsubota M, Akiyama T. Synthesis of copper/copper oxide nanoparticles by solution plasma. J Appl Phys. 2011; doi 10.1063/1.3610496.

[23] Kim SY, Lee IS, Yeon YS, Park SM, Song JK. ZnO Nanoparticles with Hexagonal Cone, Hexagonal Plate, and Rod Shapes: Synthesis and Characterization. Bull Korean Chem Soc. 2008; 29: 1960-1964.

[24] Zhao Y, Hong JM, Zhu JJ. Microwave-assisted self-assembled ZnS nanoballs. J Cryst Growth. 2004; 270: 438-445.

[25] Tahir AA, Wijayantha KGU. Photoelectrochemical water splitting at nanostructured $ZnFe_2O_4$ electrodes. J Photochem Photobiol A Chem. 2010; 216: 119-125.

[26] Lei A, Qu B, Zhou W, Wang Y, Zhang Q, Zou B. Facile synthesis and enhanced photocatalytic activity of hierarchical porous ZnO microspheres. Mater Lett. 2011; 66: 72-75.

[27] Kansal SK, Ali AH, Kapoor S, Bahnemann DW. Synthesis of flower like zinc oxide nanostructure and its application as photocatalyst. Sep Purif Technol. 2011; 80: 125-130.

[28] Fujimoto S, Tsuchiya H. Semiconductor properties and protective role of passive films of iron base alloys. Corros Sci. 2006; 49: 195-202.

[29] Kumada M, Shinoda K, Kobuchi S, Niwa K, Yamada T. Photocatalystic Effect of Rust on Acid Rain Corrosion of Carbon Steel. J Soc Mat Sci Japan. 1999; 48: 1239-1243.

[30] Tsuchiya H, Fujimoto S, Chihara O, Shibata T. Semiconductive behaviour of passive films formed on pure Cr and Fe-Cr alloys in sulfuric acid solution. Electrochim Acta. 2002; 47: 4357-4366.

[31] Kwon SC, Fan M, Wheelock TD, Saha B. Nano- and micro-iron oxide catalysts for controlling the emission of carbon monoxide and methane. Sep Purif Technol 2007; 58: 40-48.

[32] Tahir AA, Wijayantha KGU, Saremi-Yarahmadi S, Mazhar M, McKee V. Nanostructured α-Fe_2O_3 Thin Films for Photoelectrochemical Hydrogen Generation. Chem Mater. 2009; 21: 3763-3772.

[33] Boumaza S, Boudjemaa A, Omeiri S, Bouarab R, Bouguelia A, Trari M. Physical and photoelectrochemical characterizations of hematite α-Fe_2O_3: Application to photocatalytic oxygen evolution. Sol Energy. 2010; 84: 715-721.

[34] LaTempa TJ, Feng X, Paulose M, Grimes CA. Temperature-Dependent Growth of Self-Assembled Hematite (α-Fe_2O_3) Nanotube Arrays: Rapid Electrochemical Synthesis and Photoelectrochemical Properties. J Phys Chem C. 2009; 113: 16293-16298.

[35] Houas A, Lachheb H, Ksibi M, Elaloui E, Guillard C, Herrmann JM. Photocatalytic degradation pathway of methylene blue in water. Appl Catal B Environ 2001; 31: 145-157.

[36] Arvan KL, Korsunovskii GA. Variation of the absorption spectrum of methylene blue in the presence of its leuco form. Zhurnal Prikladnoi Spektroskopii. 1972; 17: 722-724.

[37] Pekakis PA, Xekoukoulotakis NP, Mantzavinos D. Treatment of textile dyehouse wastewater by TiO_2 photocatalyst. Water Res. 2006; 40: 1276-1286.

[38] Di Mondo D, Ashok D, Waldie F, Schrier N, Morrison M, Schlaf M. Stainless steel as a catalyst for the total deoxygenation of glycerol and levulinic acid in aqueous acidic medium. ACS Catal. 2011; 1: 355-364.

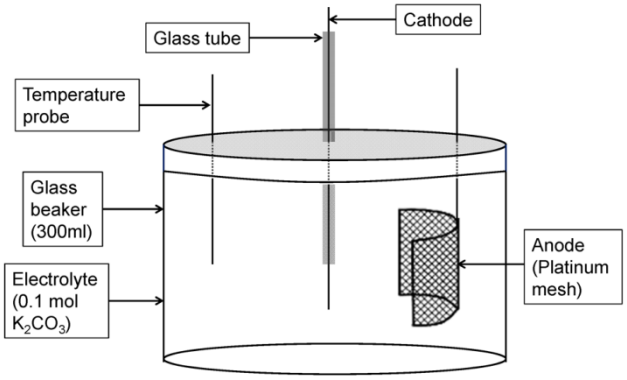

Figure 1 Schematic diagram of experimental setup for submerged glow-discharge plasma.

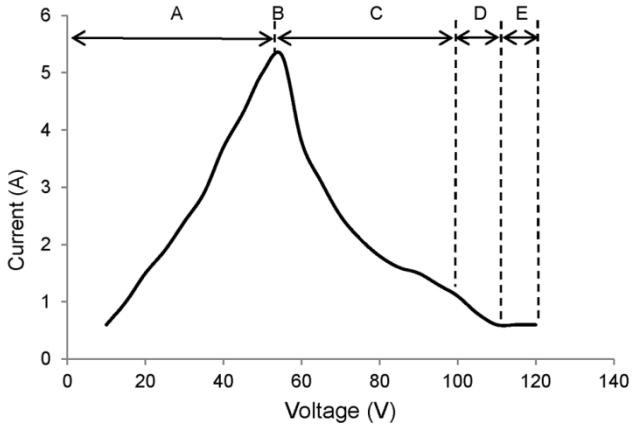

Figure 2 Voltage-current characteristics for SUS316 showing (A) conventional region, (B) breakdown point, (C) transitional region, (D) partial plasma region, and (E) glow-discharge region.

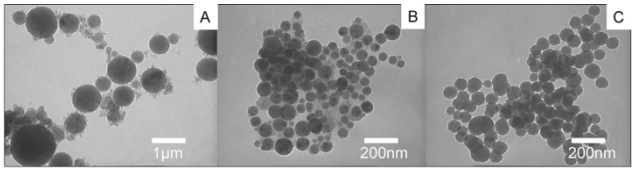

Figure 3 TEM images of (A) TiO_2, (B) ZnO and (C) SUS nanoballs.

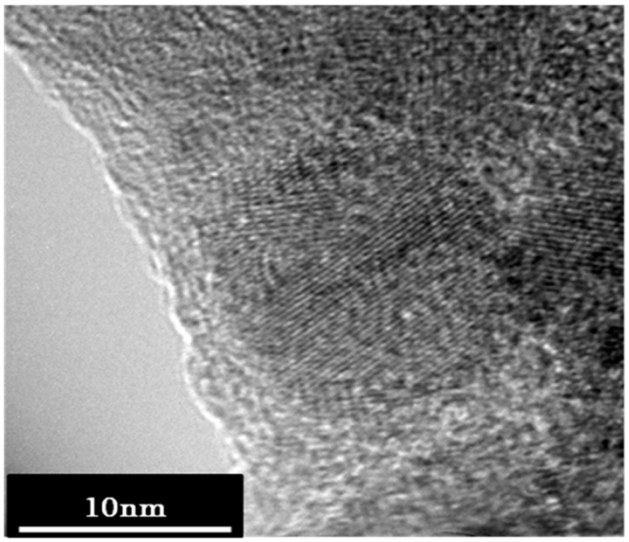

Figure 4 HRTEM image of SUS nanoballs.

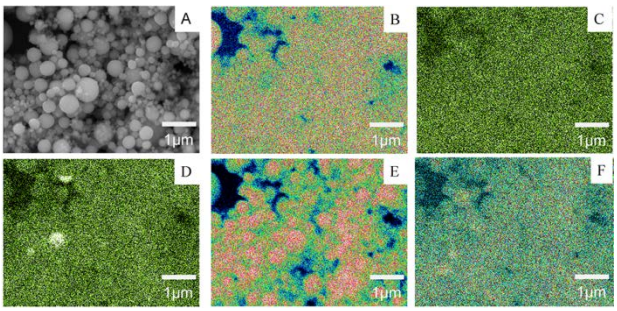

Figure 5(a) SEM-EDS map of SUS nanoballs showing (A) greyscale, (B) Fe K, (C) Mn K, (D) Ni K, (E) O K, (F) Cr K.

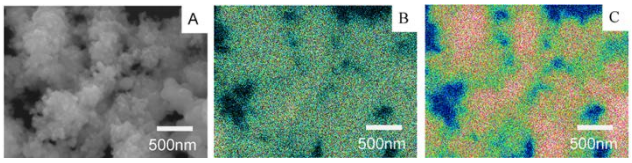

Figure 5(b) SEM-EDS map of ZnO nanoballs showing (A) greyscale, (B) Zn K, (C) O K.

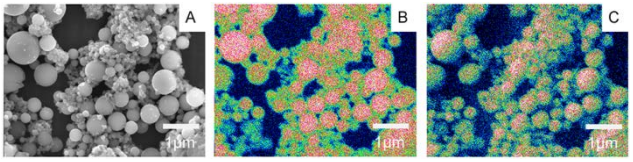

Figure 5(c) SEM-EDS map of TiO_2 nanoballs showing (A) greyscale, (B) Ti K, (C) O K.

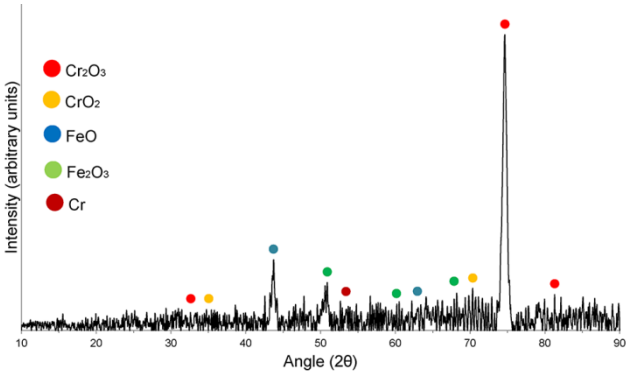

Figure 6(a) XRD spectrum of SUS nanoballs.

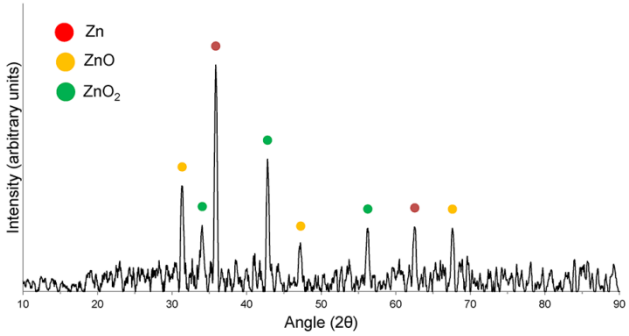

Figure 6(b) XRD spectrum of ZnO nanoballs.

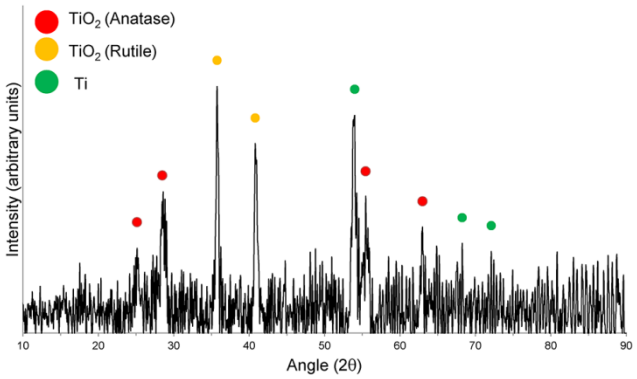

Figure 6(c) XRD spectrum of TiO_2 nanoballs.

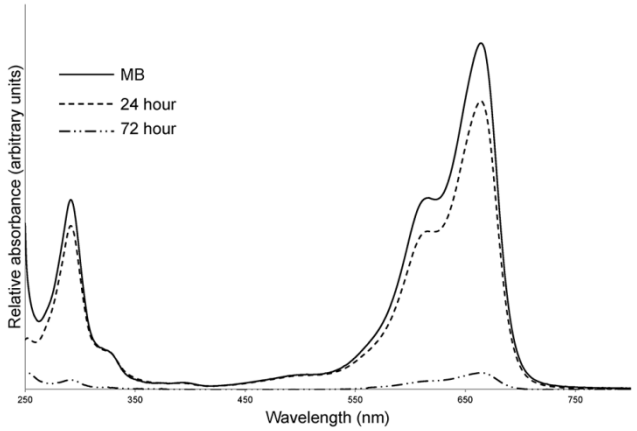

Figure 7(a) Photoabsorbance results for MB decomposition in presence of SUS nanoballs.

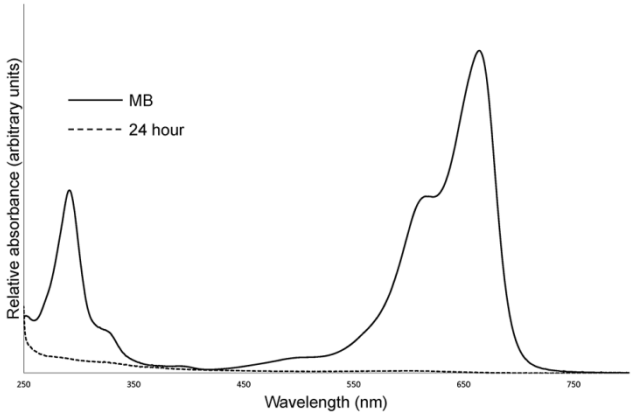

Figure 7(b) Photoabsorbance results for MB decomposition in presence of ZnO nanoballs.

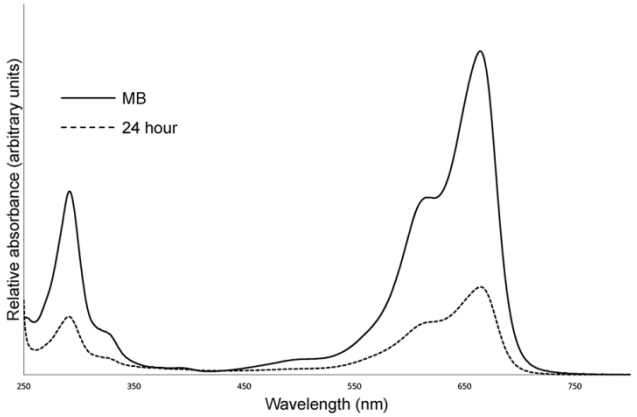

Figure 7(c) Photoabsorbance results for MB decomposition in presence of TiO_2 nanoballs

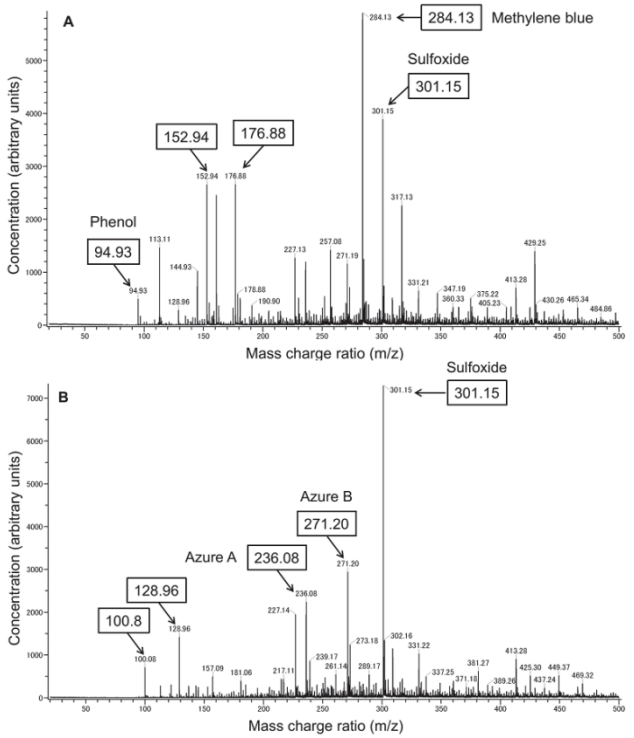

Figure 8(a) Mass spectrometry of MB after (A) 6 hours and (B) 24 hours of UV-irradiation in presence of SUS nanoballs.

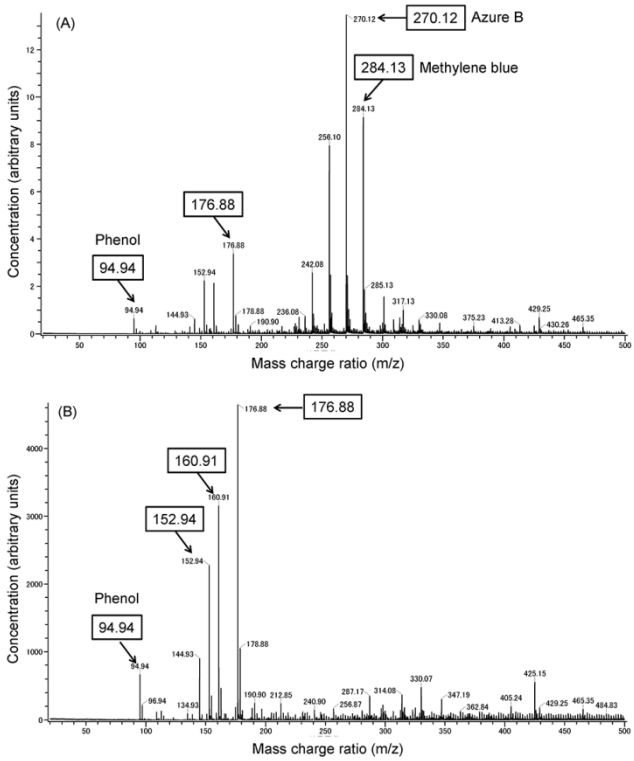

Figure 8(b) Mass spectrometry of MB after (A) 6 hours and (B) 24 hours of UV-irradiation in presence of ZnO nanoballs.

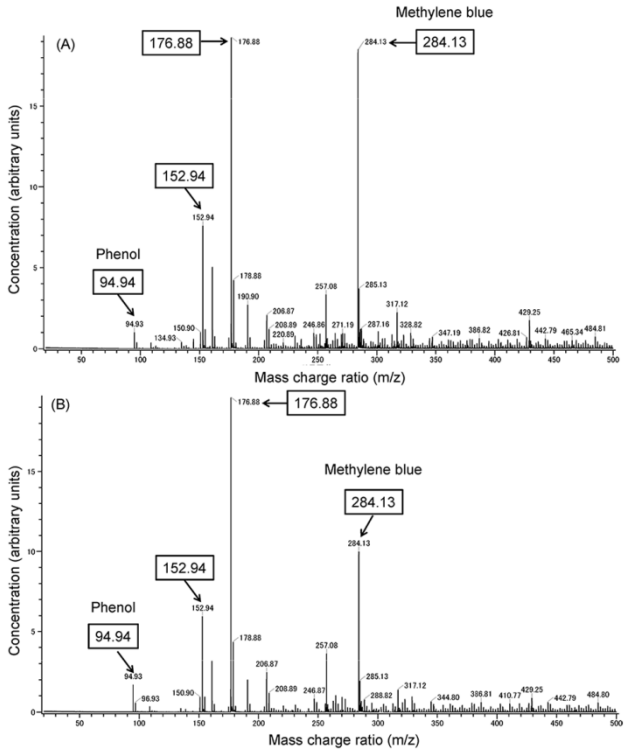

Figure 8(c) Mass spectrometry of MB after (A) 6 hours and (B) 24 hours of UV-irradiation in presence of TiO_2 nanoballs.

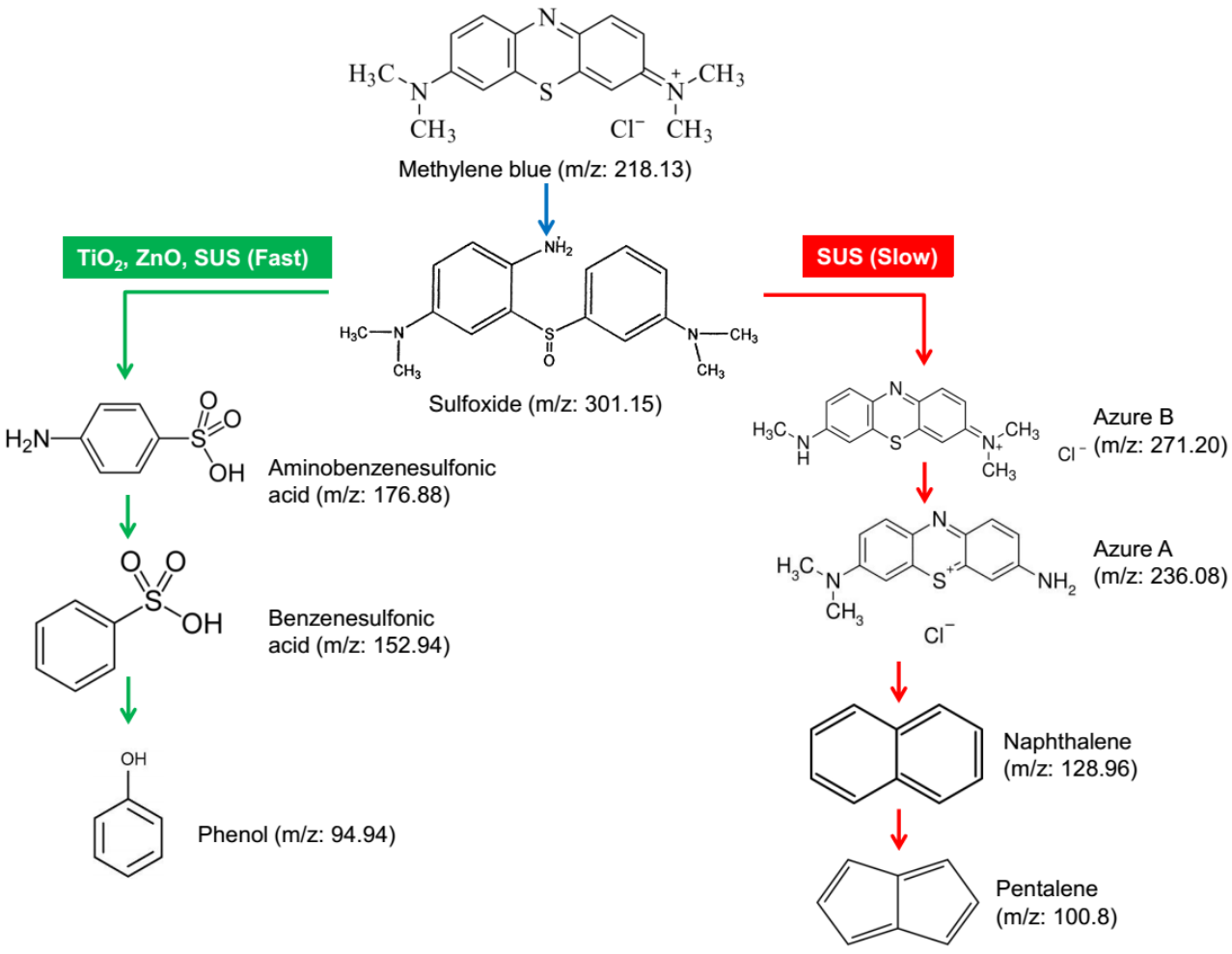

Figure 9 Proposed mechanism of MB decomposition in presence of TiO_2, ZnO and SUS nanoballs.